PF0610, a Novel Winged Helix−Turn−Helix Variant Possessing a Rubredoxin-like Zn Ribbon Motif from the Hyperthermophilic Archaeon, *Pyrococcus furiosus*[†,‡]

Xu Wang,[§] Han-Seung Lee,[§] Frank J. Sugar,[||] Francis E. Jenney, Jr.,[||] Michael W. W. Adams,[||] and James H. Prestegard*[,§]

Complex Carbohydrate Research Center, University of Georgia, Athens, Georgia 30602, and Department of Biochemistry and Molecular Biology, University of Georgia, Athens, Georgia 30602

Received September 8, 2006; Revised Manuscript Received November 16, 2006

ABSTRACT: PF0610, a protein from the hyperthermophile *Pyrococcus furiosus*, has homologues only in other archaeal species and in three species of Fe(III)-reducing bacteria. It is thought to have a helix−turn−helix (HTH) domain at the N-terminus and possesses two CXXC motifs characteristic of metal binding proteins. We have determined the solution structure of the Zn-bound protein using NMR. PF0610 is a novel winged helix−turn−helix (wHTH) protein with a rubredoxin-like Zn ribbon as its W1 segment. In addition, it possesses a large number of basic residues on its surface. Clusters of basic residues can be found on both helix H3 and the metal-binding loops of W1, suggesting that it might be a DNA-binding protein. Accordingly, gel shift assays using both linear and circular DNA showed that PF0610 does bind DNA, at least in a sequence-independent fashion. Modeling the PF0610−DNA interaction based on other wHTH protein−DNA structures revealed that besides helix H3, basic residues around the second CXXC motif in the metal-binding loop could make extensive contacts with DNA. However, the bulkiness of the W1 region implies that the DNA conformation may be distorted upon PF0610 binding. PF0610 is the first protein known to have a Zn ribbon-embedded wHTH fold and, as such, has potential roles both as a metal-dependent transcription regulator and as a component of the chromosome packing system in *P. furiosus*. The discovery of this novel structure represents the addition of another branch to the winged HTH protein family and could contribute to our understanding of transcription regulatory processes in *P. furiosus*.

Correct assignment of protein function can be pursued through biochemical studies, but structure determination can also provide insight into function. As a part of the first phase of the protein structure initiative (*1*), several of the authors of this work were involved in a structural genomics project with a special emphasis on metal-binding proteins and particularly on proteins from the hyperthermophilic archaeon, *Pyrococcus furiosus* (*2*). Approximately 30% of proteins encoded by typical genomes contain sequences suggesting metal binding activity, and metal-binding proteins span an appreciable amount of the functional space. They are known to be involved in redox chemistry, metal transport, regulatory and/or signaling functions, and simple structural stabilization. The classification of *P. furiosus* as a hyperthermophile and an archaeon also makes the study of its proteins particularly interesting. The fact that it thrives at extreme temperatures offers some advantage in terms of protein stability and ease of isolation, as well as allowing analysis by NMR at higher temperatures. In addition, *P. furiosus* is an organism with a small, well-defined genome (approximately 2200 genes) that shares roots with both prokaryotic and eukaryotic kingdoms (*3*). Here we present a NMR structure for a novel and previously uncharacterized protein from *P. furiosus* (PF0610) that has interesting metal binding properties and possibly a function connected to DNA binding.

The predicted sequence of PF0610 contains 97 amino acids corresponding to a molecular mass of 11.2 kDa. The sequence also reveals a potential Zn ribbon motif with two CXXC sequence elements near the C-terminus and an identifiable helix−turn−helix (HTH)[1] motif, which is often involved in DNA binding. These two separate motifs have resulted in the inclusion of PF0610 in two separate Pfam-B families, 12145 and 13728, as well as its tentative annotation as a transcription regulator with fused HTH and Zn ribbon domains. While structural models for the separate motifs exist, the mode of structural integration is unclear. The full sequence of PF0610 shows homologues only in archaea and three strains of Fe(III)-reducing bacteria; no structural or functional information about any of these is available. A BLAST search (*4*) reveals that no structure in the Protein

[†] This research was supported in part by a grant (GM 60329 to M.W.W.A.) from the National Institutes of Health and in part by the Protein Structure Initiative of the National Institutes of Health (GM062407 and GM074958).

[‡] Atomic coordinates of the PF0610 structure are deposited in the Protein Data Bank as entry 2GMG. Atom resonance assignments, NOESY peak lists, and RDC values are deposited in BMRB as entry 7074.

* To whom correspondence should be addressed. E-mail: jpresteg@ccrc.uga.edu. Phone: (706) 542-6281. Fax: (706) 542-4412.

[§] Complex Carbohydrate Research Center.

[||] Department of Biochemistry and Molecular Biology.

[1] Abbreviations: HTH, helix−turn−helix; wHTH, winged helix−turn−helix; GH5, globular domain of linker histone H5; RDC, residual dipolar coupling; EtBr, ethidium bromide; ICP, inductively coupled plasma.

10.1021/bi061870h CCC: $37.00
Published on Web 12/29/2006

Table 1: Parameters for NMR Experiments

experiment	nuclei[a]	^{1}H frequency (MHz)	t_1 points	t_2 points	t_3 points	F1 SW (Hz)	F2 SW (Hz)	F3 SW (Hz)	mixing time (ms)
HNCACB	^{13}C, ^{15}N, ^{1}H	600	71	32	512	8000	12062	2200	
CBCACONNH	^{13}C, ^{15}N, ^{1}H	600	71	32	512	8000	12062	2200	
HCCHTOCSY	^{13}C, ^{13}C, ^{1}H	600	70	36	683	8000	8000	12062	15.6
HC_CO_NH	^{1}H, ^{15}N, ^{1}H	600	62	32	512	8000	8000	2200	12.1
^{15}N-edited TOCSY-HSQC	^{1}H, ^{15}N, ^{1}H	600	46	32	684	8000	8000	2500	50
^{15}N-edited NOESY-HSQC	^{1}H, ^{15}N, ^{1}H	600	84	32	1024	8000	8000	12062	90
^{13}C-edited NOESY-HSQC	^{1}H, ^{13}C, ^{1}H	800	72	35	955	11204	11195	16090	90
aromatic ^{13}C-edited NOESY-HSQC	^{1}H, ^{13}C, ^{1}H	800	63	13	512	12001	6033	8000	90
^{13}C-F1-filtered F3-edited NOESY-HSQC	^{1}H, ^{13}C, ^{1}H	800	64	33	1024	9612	8000	16090	100
IPAP-HSQC	^{15}N, ^{1}H	600	128	512		8000	2200		
gNHSQC (T_2)	^{15}N, ^{1}H	600	128	512		8000	2200		
gHN_JNCo	^{15}N ,^{1}H	600	192	512		8000	2200		

[a] The nucleus acquired during each evolution time; e.g., ^{15}N, ^{1}H indicates ^{15}N is acquired during t_1 and ^{1}H is acquired during t_2.

Data Bank (PDB) (*5*) is more than 50% similar in sequence with PF0610 (*E* values of <0.87 and an alignment length of 97), and threading programs such as mGenTHREADER (*6*) show PF0610 has no structural similarities with any members of the PDB (*p* values of <0.033). Hence, PF0610 was regarded as a viable structural genomics target, and its structure determination was continued under the auspices of the Northeast Structural Genomics Consortium (*7*). NMR was chosen as an approach to structure determination given the modest size of the protein and its failure to crystallize in the initial screening. We report here the structure of PF0610 determined using NMR techniques along with experimental tests of function suggested on the basis of its structure.

EXPERIMENTAL PROCEDURES

Protein Expression and Purification. The open reading frame of PF0610 was cloned into a modified pET-24d expression vector with an N-terminal six-His tag, resulting in the insertion of the AHHHHHHGS sequence into the N-terminus of the PF0610 protein. The protein was expressed in *Escherichia coli* strain BL21(DE3)pRIL. ^{15}N and ^{13}C isotopic labeling of the protein was accomplished by growing cells in M9 medium supplemented with ^{15}N-labeled NH_4Cl and ^{13}C-labeled D-glucose. Because the CXXC motifs can bind Fe^{2+} and Fe^{3+} which are deleterious to NMR spectra, the media were also supplemented with 20 μM $ZnSO_4$ to produce a Zn^{2+}-loaded protein. The cells were grown at 37 °C to an OD_{600} of ~0.8−1.0 before induction with 0.5 mM IPTG. The cells were harvested and lysed 18 h after the induction at 18 °C. The supernatant of the lysate was applied to a Ni-NTA column (Qiagen) equilibrated with a 500 mM NaCl, 20 mM phosphate buffer at pH 8.0. After the protein was eluted off the column with 300 mM imidazole, it was concentrated using an Amicon Ultra centrifugal concentrator with a molecular mass cutoff of 5 kDa and applied to a strong cation exchange column (SP Sepharose, GE Healthcare). The protein was eluted with a NaCl gradient from 0 to 1 M salt. The eluted protein was further purified using a Superdex 75 gel filtration column (GE Healthcare) equilibrated with 20 mM Tris (pH 8.0) and 300 mM NaCl. The purified protein was then buffer exchanged against 20 mM Tris (pH 8.0) and 100 mM NaCl. The metal content of the protein was determined by ICP spectroscopy at the Chemical Analysis Laboratory of the University of Georgia. NMR samples typically contain 100 mM NaCl, 20 mM Tris (pH 8.0), 2 mM DTT, 10% D_2O, and ~0.4 mM PF0610. Attempts to prepare samples with higher concentrations of PF0610 resulted in significant precipitation.

Sedimentation Equilibrium Studies. Sedimentation equilibrium experiments were conducted on a Beckman Optima XL-A (Beckman Coulter, Fullerton, CA) analytical ultracentrifuge, with a four-position AN-60-Ti rotor. Metal-loaded PF0610 was prepared in 20 mM Tris-HCl (pH 8.0) and 50 mM NaCl and centrifuged in six-sector Epon/charcoal centerpieces. Three different concentrations (14, 35, and 55 μM) of PF0610 were analyzed with absorbance readings of 0.1, 0.25, and 0.4 optical density unit at 280 nm ($\epsilon_{280} = 7240$ M^{-1} cm^{-1}). Experiments were performed at 20 °C and at three speeds ranging from 24 000 to 40 000 rpm. Scans were collected in a radial increment mode with 0.001 increments and four-point averaging. The samples were allowed to equilibrate for 24 h prior to the recording of the scan. The data were fit using Ultrascan 7.0 (www.ultrascan.uthscsa.edu).

NMR Data Collection and Processing. All NMR spectra, with the exception of the ^{13}C-edited NOESY-HSQC spectra, were recorded on a Varian Inova 600 MHz spectrometer equipped with a triple-resonance cryogenic probe. The ^{13}C-edited NOESY-HSQC spectra were collected on a Varian Inova 800 MHz spectrometer also equipped with a triple-resonance cryogenic probe. All data were collected at 25 °C using pulse sequences from the BioPack package distributed by Varian Inc. For backbone assignment, data from the CBCACONNH and HNCACB experiments were used. Any remaining ambiguities were resolved with a combination of HCCONH and ^{15}N-edited TOCSY-HSQC experiments. Side chain assignments were made using the HCCHTOCSY experiment. For structure calculation, ^{15}N-edited NOESY-HSQC and ^{13}C-edited NOESY-HSQC experiments for both the aliphatic and aromatic regions were collected. NH, NC, and HC residual dipolar couplings (RDCs) were measured by aligning the protein in a liquid crystalline medium consisting of a 4% (w/v) pentaethylene glycol monododecyl ether ($C_{12}E_5$)/hexanol mixture in aqueous buffer with an approximate $C_{12}E_5$:hexanol molar ratio of 1. The ^{15}N IPAP-HSQC experiment was used to collect $^1J_{NH}$, and the two-dimensional gHN_Jnco experiment (*8*) was used to measure $^1J_{NC}$ and $^2J_{HNCO}$. Table 1 lists detailed parameters for all NMR experiments. The ^{15}N T_2 relaxation data were acquired using the gNhsqc pulse sequence from Biopack with a variable delay of 10, 30, 50 70, 90, or 110 ms before the ^{15}N

evolution. Chemical exchange contributions to the ^{15}N T_2 values were measured using the relaxation-compensated CPMG pulse sequence with a τ_{cp} time of 1 and 21.5 ms (*9*, *10*). All data were processed with NMRPipe (*11*) and analyzed using NMRView (*12*). SmartNoteBook (*13*) was also used to aid the backbone assignment process.

Structure Calculation. Backbone dihedral angle restraints were derived from chemical shift information using TALOS (*14*). The TALOS output was also compared with experimentally measured $^3J_{HNHA}$. Only restraints that concur in both measurements were used. Cross-peaks in the NOESY experiments were first assigned manually to produce a total of 178 NOE assignments, of which 31 were long-range. The partially assigned lists were then used as the input for the automatic NOE assignment script in CYANA (*15*, *16*). The 50 best structures from the CYANA calculation were subsequently refined using XPLOR-NIH (*17*) following the default refinement procedure. Besides the 923 NOE-derived distance restraints calculated with CYANA and 55 ϕ and 53 ψ dihedral angle restraints, 72 NH RDCs, 69 NC RDCs, and 67 HNCO RDCs were also used in the refinement process. Four pseudodistance restraints of 2.3 Å were added between the Zn atom and the deprotonated side chain sulfur atoms of the cysteines during XPLOR-NIH refinement. These distances were obtained using the average S−Fe distances found in the crystal structure of Pf rubredoxin (*18*). No explicit solvent refinement was carried out during refinement.

Gel Shift Assays. On the basis of the annotation of PF0610 as a potential transcription factor, we screened for possible DNA target sequences of PF0610 using 5′ noncoding segments close to the PF0610 gene. The 200 bp fragment in the 5′ region of PF0605 and PF0606 (IG1) was amplified with primers 5′-tgattacttccctgcgagtg-3′ and 5′-aagacgttccaacttcttcc-3′. The 180 bp fragment in the 5′ region of the PF0607 gene (IG2) was amplified with primers 5′-aacgataatgaacatgacgg-3′ and 5′-cgctactatgccagtggaag-3′. The 190 bp fragment in the 5′ region of the PF0608 gene (IG3) was amplified with primers 5′-gaaggtctacaacaaatttg-3′ and 5′-gattaaagccctctcgaacc-3′. The 200 bp fragment from the 5′ region of the PF0610 and Pf0611 genes (IG4) was amplified with primers 5′-ctaaaatcctcgctagctca-3′ and 5′-cattctattggccaaccaag-3′. In the gel shift assay, 140 ng of each fragment was mixed with 50 μg of PF0610 in a 20 mM Tris (pH 8.0), 100 mM NaCl buffer and incubated at 55 °C for 30 min before application to the 2% agarose gel for electrophoresis. In the titration of linear and circular DNA with PF0610, either 0.5 μg (final concentration of 0.39 μM) aliquots of IG1 fragment or 0.5 μg (final concentration of 0.03 μM) aliquots of circular pDONR221 plasmid was mixed with 0.125, 0.25, 0.5, 1, and 2 μg of PF0610 (final concentrations of 1.15, 2.3, 4.6, 9.2, and 18 μM, respectively) in the aforementioned buffer and incubated at 55 °C for 30 min before application to either a 2 or 1.2% agarose gel for electrophoresis. To examine the effect of buffering reagents and pH on the solubility of the protein−DNA complex, six different buffer solutions containing 20 μM PF0610 and 0.5 μM IG1 fragment were prepared. Each solution was tested for the presence of precipitant and analyzed using agarose gel electrophoresis for the presence of the protein−DNA complex. The six buffers follow: (1) 20 mM Tris and 50 mM NaCl (pH 8.0), (2) 20 mM and 1 mM EDTA (pH 8.0), (3) 20 mM BisTris and 50 mM NaCl (pH 6.5), (4) 20 mM phosphate and 50 mM NaCl (pH 6.8), (5) 20 mM MES and 50 mM NaCl (pH 6.5), and (6) 20 mM MES and 100 mM NaCl (pH 6.5).

It should be noted that the numbering system used herein for the amino acid residues of PF0610 refers to the recombinant form of the protein, which has a nine-residue His tag at the N-terminus. This replaces the N-terminal Met of the native protein. Therefore, correspondence between the wild-type sequence and the recombinant sequence can be obtained by an addition of eight to the wild-type sequence numbering. PF0610 is also a target for the Northeast Structural Genomics Consortium (www.nesg.org) and bears the NESG target number of Pfg3.

RESULTS

Metal Saturation State of PF0610. The expression level of PF0610 in *E. coli* grown in M9 medium was modest with 1 L of culture yielding approximately 1.3 mg of protein that was homogeneous as determined by SDS−PAGE analysis. As a recombinant protein expressed in *E. coli*, PF0610 can bind both Zn and Fe. PF0610 expressed in normal M9 medium containing Fe and Zn ions (10 μM each) had a Fe content of approximately 0.8 ± 0.1 mol of Fe/mol of PF0610. The Zn content in these proteins was negligible (<0.1 mol of Zn/mol of PF0610). However, when cells were grown in a medium supplemented with 30 μM Zn (the Fe concentration remained at 10 μM), purified PF0610 contained 0.8 mol of Zn/mol of PF0610 and the Fe content was negligible. The visible spectrum of the Fe-containing protein (data not shown) indicated the presence of an [FeS_4] rubredoxin-like center (*19*). It is therefore assumed that the metal ion in the recombinant protein is coordinated by the four cysteinyl residues in a tetrahedral arrangement. The metal binding motif in PF0610 will therefore be termed the Zn ribbon motif, although the name only implies the existence of a distinct three-β-strand fold of the type found in rubredoxin-like proteins, and the motif is capable of binding a variety of metal ions other than Zn. The metal ion in recombinant PF0610 is tightly bound as the metal content remained unchanged when the Zn-containing protein was incubated (25 °C and pH 8.0) with up to 200 mM EDTA. However, it is important to emphasize that the metal content of native PF0610 in *P. furiosus* is unknown.

Because the additional nuclear relaxation effect induced by the paramagnetic Fe ion degrades the NMR signal, we have chosen to work predominantly with the Zn form of the protein. The structural effects of various metal substitutions in Zn ribbon proteins have been thoroughly studied (for a case study on rubredoxin, see ref *20*), and there is no evidence of significant structural perturbation when Fe is exchanged for Zn in these proteins. Therefore, irrespective of the metal saturation state of PF0610 in vivo, the structure determined in this study should be an accurate representation of the functional form of the protein.

Dimerization and Sedimentation Equilibrium Study of PF0610. During the purification of the protein, its elution from the Superdex 75 gel filtration column indicated a molecular mass of ~25 kDa, suggesting that it is a dimer at pH 8.0 rather than a monomer. NMR relaxation studies of the protein at higher concentrations (>0.3 mM) also revealed that its transverse relaxation time (~60 ms) was shorter than would be expected for a protein of 12.3 kDa, further implying

the molecular mass of PF0610 in solution is larger than its monomeric mass. To accurately determine the extent of dimerization, an analytical ultracentrifugation study of the protein was conducted. Three different concentrations of the protein were centrifuged at three different speeds in accumulating nine sets of data, which were then averaged on the basis of the speed and fitted to absorbance curve using the monomer−dimer equilibrium model (Figure 2a). The sedimentation equilibrium data showed the K_d of dimerization is ~450 μM [in 20 mM Tris (pH 8.0) and 100 mM NaCl]. This implies that at a concentration of 0.5 mM, only 40% of the protein exists in the dimer form (Figure 2b). Since all of the NMR data were collected using samples with protein concentrations of only 0.4 mM, only ~30% of the protein exists as dimers, and (if we assume slow exchange) much higher signal intensities are expected from monomers, NOE data should be dominated by the monomeric form of the protein. Nevertheless, an attempt was made to detect and differentiate the intermolecular NOEs from the intramolecular ones using a mixed sample containing half ^{13}C-labeled protein and half ^{12}C-labeled protein. The ^{13}C-F3-edited/F1-filtered NOESY-HSQC spectrum acquired using the sample revealed no intermolecular NOE cross-peaks. These observations confirmed that the NOE cross-peaks used to derive the distance restraints in the structure calculations originated entirely from monomeric proteins. Whether the weak dimerization of PF0610 has any biological relevance is unclear.

Structure of Zn-Bound PF0610. Figure 3a shows an ensemble of the 10 lowest-energy structures of a total of 50 calculated in the refinement process. This ensemble of PF0610 structures has an overall backbone rmsd of 0.6 Å for the well-defined region of the protein (residues 11−33, 41−88, and 93−104). The protein structure converged quickly in CYANA calculations to a backbone rmsd of ~1.1 Å with 81% of backbone dihedral angles in the most favored region of the Ramachandran plot. RDC-assisted refinement using XPLOR-NIH decreased the backbone rmsd even further, and the backbone dihedral angle distribution also improved to 93% in the most favored region of the Ramachandran plot. Although pseudodistance restraints between Zn and sulfur of the cysteines were used in the refinement process, the conformations of the metal binding loops were already very well defined in CYANA calculations, where they are not used. Table 2 lists other structural statistics for this ensemble.

The PF0610 structure closely follows the canonical wHTH fold (see Figure 1 for the nomenclature of the wHTH fold). The three helices are arranged in a half-open bundle similar to other wHTH motifs (*21*, *22*). The long eight-residue linker between H2 and H3 is a hallmark of wHTH proteins that distinguishes them from HTH motifs, which usually has an only three-residue linker connecting H2 and H3. The interhelical angle between H2 and H3 of PF0610 is ~100°, similar to that of the wHTH protein BirA, but different from the majority of those of HTH proteins, whose H2−H3 helices hold at a constant angle of ~120° (*22*). The N-terminus of the protein is composed of three-turn helix H1. Its helical axis is almost perpendicular to the plane of the twisted β-sheet. The hydrophobic side of the helix, made up of residues I16, I17, and L20, contributes to the formation of the hydrophobic core of PF0610 (Figure 4a). The linker between H1 and H2 adopts an extended β-strand-like conformation along the C-terminal β-strand. The two segments are linked by extensive hydrophobic contacts between residues L20, L21, and G24 in the linker and C-terminal residues F100 and L102. The longest helix in PF0610 is the H3 helix. It possesses five turns and lies diagonally against the β-sheet. Four hydrophobic residues in the helix (I45, I52, L46, and L49) make up part of the hydrophobic core (Figure 4a). H3 is also the DNA recognition helix in the canonical wHTH structure. H3 of PF0610 possesses six basic residues (K42, K43, K50, K54, K57, and R58) and three acidic residues [E47, D48, and E59 (Figure 4b)]. This distribution of charged side chains makes it a strong candidate for DNA interaction. As with other wHTH proteins, the half-open hydrophobic core of the trihelical bundle is closed from the solvent by a two-stranded β-sheet. Residues L63, I65, F100, and L102 of the β-sheet form part of the core with the side chain of M61 on the fringe of the core. There is also a cluster of basic residues on the solvent-accessible side of the β-sheet formed by K66, R99, and K101. This raises the possibility that the β-sheet may also be involved in DNA interactions. Each strand of the antiparallel sheet contains eight residues, longer than β-hairpins found in the majority of wHTH proteins. The length of the strands in PF0610 is the result of the most unique feature of PF0610, a W1 segment possessing regular secondary structural elements.

Table 2: Summary of Structural Statistics of the Ensemble of 10 (of a total of 50 calculated) PF0610 Solution Structures

no. of NOE-derived distance restraints	
short-range ($\|i-j\| < 2$)	310
medium-range ($2 \le \|i-j\| < 5$)	235
long-range ($\|i-j\| > 5$)	378
total	923
no. of backbone dihedral angle restraints	
φ	55
ψ	53
RDC	
NH	72
NC	69
HNCO	67
axial component	-9.1 ± 0.1 Hz
rhombicity	0.6 ± 0.1
rmsd	
backbone	0.8 Å,[a] 0.6 Å[b]
all heavy atoms	1.2 Å,[a] 1.0 Å[b]
no. of distance restraint violations >0.5 Å	0
no. of dihedral angle violations >10°	0
backbone dihedral angle distribution	
% in most favored regions	93.2
% in additionally allowed regions	6.8
% in other regions	0

[a] For all residues. [b] For the well-defined region, defined as any region with a backbone dihedral angle order parameter greater than 1.8. In the case of PF0610, this includes residues 11−33, 41−88, and 93−104.

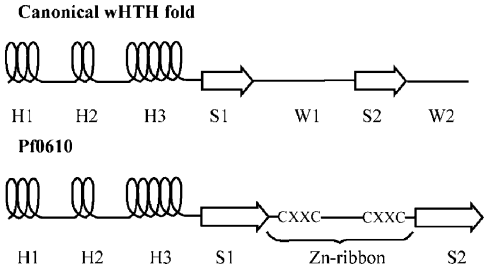

FIGURE 1: Schematic topologies of the canonical wHTH protein and PF0610. The nomenclature of each segment in the protein is also illustrated.

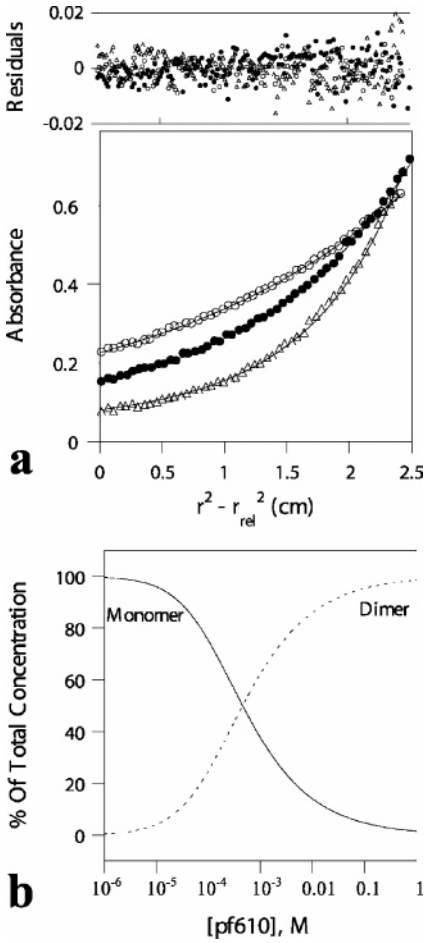

FIGURE 2: Results of the sedimentation equilibrium study of PF0610. (a) Global fitting of the sedimentation equilibrium data. The equilibrium data are fit best to a monomer−dimer equilibrium model, resulting in the monomer molecular weight and the dimer association constant. The absorption data at 280 nm and the residuals from the monomer−dimer fits are shown. These experiments were conducted at protein concentrations of 14, 35, and 55 μM and at speeds of 24 000 (○), 30 000 (●), and 40 000 rpm (△). (b) Monomer−dimer fractions determined from the association constant from sedimentation equilibrium experiments.

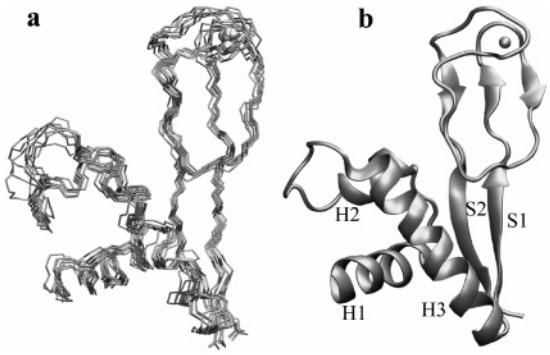

FIGURE 3: (a) Ensemble of 10 lowest-energy PF0610 solution structures from a total of 50 calculated structures. Only residues 10−105 are shown. (b) Ribbon schematic diagram of the Pf0610 structure. In both panels, Zn ions are shown as spheres.

The W1 component in most wHTH proteins is a short loop (<10 residues) with no secondary structure (*21*−*23*). The only wHTH protein known to possess a W1 segment as long as PF0610 is the *E. coli* protein yhgG (PDB entry 1XN7). The solution structure of yhgG revealed that its W1 segment is also a flexible loop (loop rmsd of >6.5 Å after superimposing the HTH motif) with no secondary structure. The W1 region in PF0610, on the other hand, forms a well-defined rubredoxin-like Zn ribbon fold. The Zn ribbon motif has been known to exist in HTH proteins, but usually as an independent domain (*21*, *24*). However, the Zn ribbon in PF0610 is an integral part of the wHTH fold. In the PF0610 structure, strand 1 (S1) of PF0610 is continued until the formation of a tight CXXC turn that makes up half of the metal chelating cluster. This is followed by a short antiparallel β-hairpin-like structure, a loop containing the second CXXC motif, and, finally, the C-terminal β-strand. The arrangement of Cys side chains in the metal-binding loop of PF0610 is similar to that of *P. furiosus* rubredoxin (*25*). The conformations of the turn and loop containing the two CXXC motifs are almost identical to that of rubredoxin (Figure 5a). The positioning of secondary structural elements around the metal binding loop is also similar. Residues 66−70, 75−78, and 94−97 correspond to the three β-strands in rubredoxin, while residues 82−86 match the fourth β-sheet-like structure in rubredoxin. The main difference between the two is in the length of the loop between the two CXXC motifs. Rubredoxin has 29 residues between the CXXC motifs, whereas the two CXXC motifs in PF0610 are separated by only 13 residues. This discrepancy is reflected in the much better agreement between PF0610 and the first two β-strands of rubredoxin than between PF0610 and the β-like structure plus the last β-strand in rubredoxin. Another difference between them is in the charge distribution of the metal-binding loops. PF0610 has five basic residues (R71, K72, R86, K89, and K91) surrounding its two CXXC motifs, creating a high concentration of positive charges around them (Figure 4b). Charged residues in rubredoxin, on the other hand, are predominantly acidic. This could be the result of evolutionary adaptations by PF0610 to move from a more acidic precursor that also gave rise to rubredoxin, to function as a DNA-binding protein. Another well-known Zn ribbon protein from *P. furiosus* is transcription factor TFIIB (*26*). Unlike rubredoxin, which is isolated only as a Fe-containing protein in vivo, the N-terminus of TFIIB is believed to bind predominantly Zn in vivo but can also incorporate Fe, Co, and other metals. However, the polarity of the Zn ribbon motif in TFIIB is the opposite of that of PF0610; i.e., the N-terminus of the TFIIB Zn ribbon corresponds to the C-terminus of the PF0610 Zn ribbon. Figure 5b shows the superimposition of the metal binding region of PF0610 with that of the N-terminal domain of *P. furiosus* TFIIB. As with rubredoxin, the agreements around the CXXC motifs and the β-strands are good between the two proteins. Because of the reversal of polypeptide chain polarity, the loop between the CXXC motifs is missing in TFIIB. It is noteworthy that in PF0610, the loop between the CXXC motifs is anchored to the wHTH fold by the hydrophobic contacts between residue I81 and residues L46, I65, P98, and F100 in the hydrophobic core. This fixes the orientation of the W1 domain relative to the rest of the protein.

The tight integration of the Zn ribbon domain to the wHTH domain is supported by ^{15}N T_2 data (Figure 6). The values of T_2 throughout the protein are uniformly around 60 ms. This contradicts the notion that the smaller Zn ribbon motif might be independent from the larger wHTH portion since that assumption would imply a longer T_2 time for the smaller domain. Residues 64−66 and 99−101, which are the linkers

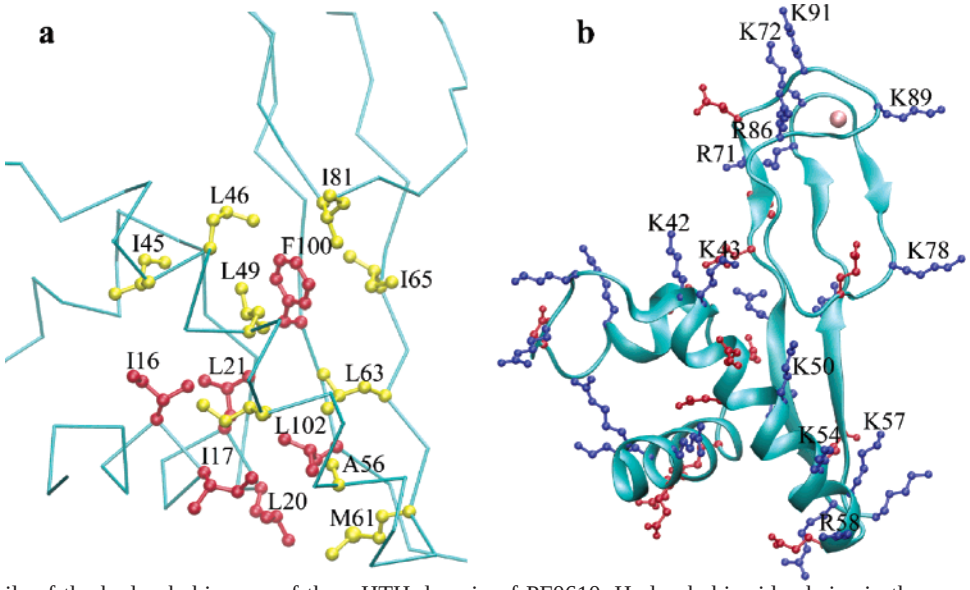

FIGURE 4: (a) Details of the hydrophobic core of the wHTH domain of PF0610. Hydrophobic side chains in the core are depicted using ball-and-stick models. The backbone Cα trace is colored cyan. For reasons of visual clarity, residues I16, I17, L20, L21, F100, and L102 are colored red and other hydrophobic residues are colored yellow. (b) Distributions of charged residues on PF0610. Lys and Arg side chains are colored blue. Asp and Glu side chains are colored red. Lys and Arg side chains that are potentially important for DNA interactions are labeled. The Zn ion is represented as a sphere.

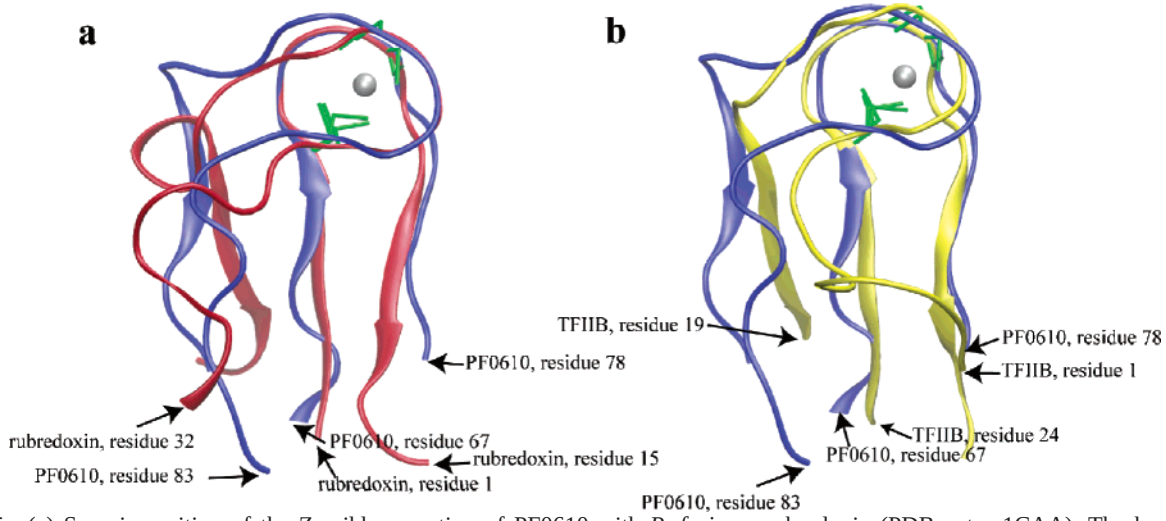

FIGURE 5: (a) Superimposition of the Zn ribbon portion of PF0610 with *P. furiosus* rubredoxin (PDB entry 1CAA). The backbone of PF0610 is colored blue, and the backbone of rubredoxin is colored red. For clarity, only residues 67−78 and 83−98 of PF0610 and residues 1−15 and 32−53 of rubredoxin are shown. (b) Superimposition of the Zn ribbon portion of PF0610 with the N-terminal domain of *P. furiosus* TFIIB (PDB entry 1PFT). The backbone of PF0610 is colored blue, and the backbone of TFIIB is colored yellow. For clarity, only residues 67−78 and 83−98 of PF0610 and residues 1−19 and 24−37 of TFIIB are shown. In both panels, the Cys side chains are colored green and the Fe in rubredoxin is shown as a sphere.

connecting the two domains, also have T_2 values that are in line with them being parts of rigid β-sheets rather than flexible linkers. To probe the presence of conformational exchange in the protein, we also performed relaxation-compensated CPMG experiments on the Zn form of PF0610 with τ_{cp} values of 1 and 21.5 ms (*9*). No difference larger than 3 s^{-1} was observed in the R_2 values measured at two times. This confirmed that the structure is rigid. Interestingly, residues V76, F77, K78, E80, and N82 in the loop between the two CXXC motifs did exhibit a small but significant difference between the R_2 values measured at the two τ_{cp} times, indicating some flexibility in this region.

DNA Interaction Assays. Because PF0610 was identified as a possible DNA binding protein by bioinformatic analysis, our initial suspicion was that it might regulate gene expression, possibly of genes that are close to the PF0610 ORF.

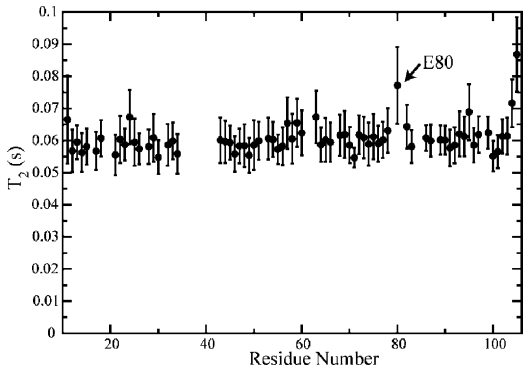

FIGURE 6: Backbone amide nitrogen T_2 values of PF0610.

Possible transcription regulatory regions for genes encoding PF0606, PF0607, PF0608, and PF0611 were amplified by

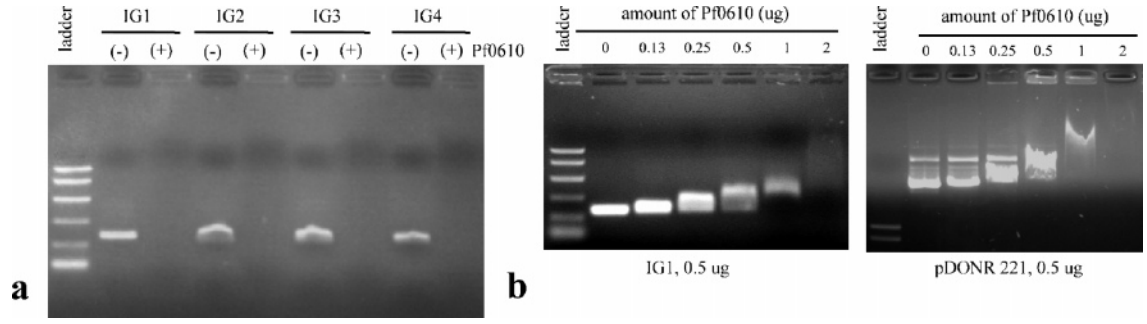

FIGURE 7: (a) Effects of PF0610 on migration of DNA fragments IG1−IG4. Note the weak fluorescence in the well of the sample with PF0610. (b) Titration of linear and circular DNA with PF0610. The upper band seen in the sample of the plasmid corresponds to the linear form of the plasmid.

PCR and used in a gel shift assay with PF0610. The results of the assay are shown in Figure 7a. Irrespective of the DNA sequence, addition of PF0610 eliminated all traces of fluorescence emitted by EtBr inserted into DNA. Careful examination showed that there is still a trace of fluorescence from the well of each lane containing PF0610, indicating DNA has been localized to the well in the presence of PF0610 and the level of binding of EtBr to DNA is greatly reduced by the presence of PF610. Subsequent results from gel shift assays with both linear and circular DNA of different sequences confirmed that PF0610 interacts with DNA in a sequence-independent manner. Figure 7b shows results from the titration of linear and circular DNA with PF0610. At low concentrations of the protein, impedance of DNA migration is clearly correlated with the concentration of the protein. The level of smearing of the DNA bands also increased with the protein concentration, implying the existence of different stoichiometries for protein−DNA complexes. At high protein concentrations, the DNA band, either linear or circular, disappears entirely from the gel, indicating that saturating binding sites prevent EtBr from inserting. To demonstrate that the disappearance of the DNA is not due to the precipitation of the protein−DNA complex, we examined the solubility of the PF0610−IG1 complex in six different buffering systems with pHs ranging from 6.5 to 8.0. At a protein concentration of 20 μM and a DNA concentration of 0.5 μM, the complex is completely soluble in all six buffers. Thus, we believe precipitation is not a cause for the disappearance of the bands at the concentrations of protein and DNA used in the assay. Both Fe-bound and Zn-bound PF0610 were utilized in these experiments, and no difference was observed between the gel shifting patterns produced by the two forms of the protein. Preliminary results of the interactions of PF0610 with the self-complementary primer 5′-CGAGATCTGAGCTTTTGCTCAGATCTCG indicate, at a protein concentration of 70 μM and a primer concentration of 400 μM, the complex is fully soluble in 20 mM phosphate (pH 8.0) and 100 mM NaCl, and the dissociation constant for the complex is on the order of micromolar.

DISCUSSION

Uniqueness of the PF0610 Fold. The HTH motif is often found in DNA-binding proteins that play crucial roles in DNA packing, replication, and transcription. The wHTH motif, a variant of the HTH motif, was first discovered in 1993 (*27*). In addition to the half-open trihelical bundle found in the HTH motif, wHTH proteins also possess a two-stranded antiparallel β-hairpin at the C-terminus. The canonical wHTH structure is flanked by two winglike loops (W1 and W2), one located between the two strands and the other at the C-terminus. These engage interactions with the more distant parts of the DNA, helping to increase the surface area of interaction and strengthening the protein's affinity for the double helix. Many variations on the number of helices and strands in the wHTH structure have since been discovered (for a review, see ref *21*). But a constant feature within this protein class is the presence of the W1 segment in an unstructured looplike conformation.

The determination of the PF0610 structure shows that a new branch exists in the wHTH family tree. PF0610 is the first wHTH protein known to have another structural motif inserted into the wHTH domain. Unlike the Zn ribbon containing wHTH transcription factors TFIIEα and TFIIB, whose Zn ribbon motifs are independent of their wHTH domains, the rubredoxin-like W1 portion of PF0610 is closely integrated with the rest of the protein. Besides the two rigid β-strand structures connecting the Zn ribbon with the wHTH domain, I81 of W1 also inserts itself into the hydrophobic core, fixing the orientation of the Zn ribbon loop relative to the wHTH domain. It is known that archaea genomes contain almost twice as many Zn ribbon proteins as bacterial genomes (*24*). The uniqueness of this Zn ribbon-embedded wHTH motif in archaea and Fe(III)-reducing bacteria is testament to the importance of metal-binding proteins to the cellular processes of archaea.

Structure of PF0610 and Its Implication for DNA Binding. Interactions of the wHTH domain with DNA have been studied well. Initial results indicated that, just like the HTH motif, H3 in wHTH proteins serves as the main recognition helix interacting with the major groove while the wings contact bases in more distant parts of DNA (*28*). A later study carried out using RFX1 revealed an additional mode of interaction between wHTH proteins and DNA. In particular, it was shown that RFX1 conferred DNA recognition through insertion of W1 in the major groove as opposed to insertion of H3. H3 was instead relegated to the minor groove, leading to an ~3 Å widening of the minor groove. wHTH proteins of this type usually have a high concentration of basic residues in the area around W1 rather than on H3. Although the majority of wHTH-containing transcription factors bind DNA in a sequence specific manner, interactions of wHTH protein with DNA need not be sequence specific. The globular domain of linker histone H5 (GH5) and the Z-DNA binding domain of the protein ADAR1 both bind DNA in a manner that is independent of the sequence.

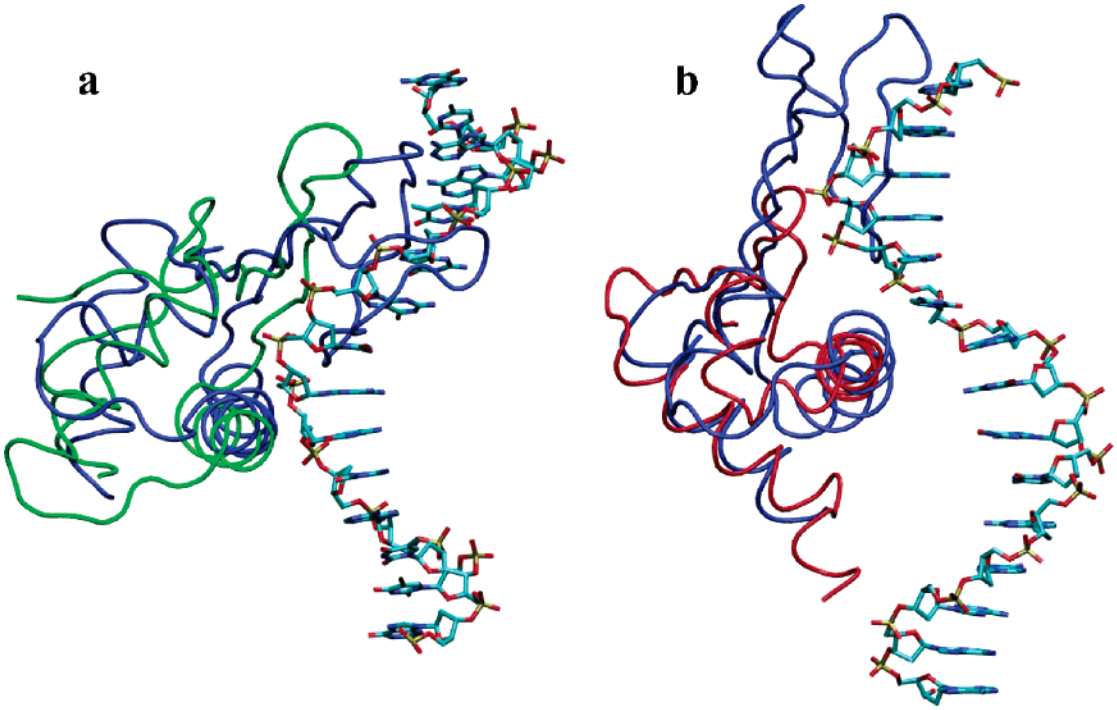

FIGURE 8: (a) Superimposition of PF0610 with RFX1 (PDB entry 1DP7). The backbone of PF0610 is colored blue, while the backbone of RFX1 is colored green. (b) Superimposition of PF0610 with DP2 (PDB entry 1CF7). The backbone of DP2 is colored red. In both diagrams, only one strand of DNA is shown.

PF0610 has several clusters of basic residues located on opposite sides of its surface. However, the question of how this attribute affects its interaction with DNA is unclear. We have modeled PF0610−DNA interaction using structures of wHTH proteins RFX1 and DP2 complexed to DNA (*29*, *30*). The DP2 protein interacts with DNA in the canonical fashion with helix H3 in the major groove, whereas RFX1 binds to the DNA atypically with H3 in the minor groove. Figure 8 shows the structure-based alignments of PF0610 with the DNA-bound RFX1 and DP2 carried out using the DALI server (*31*). The *Z* score of alignment between DP2 and PF0610 is 3.6, which is much higher than the threshold score of 2.0 and indicates a good agreement between the two structures. Because of the slightly different orientation of H1 in PF0610 and RFX1, as well as differences in the lengths of H2 and H3, the *Z* score for alignment of the two proteins is only 2.6.

Models from both scenarios revealed that the basic patch on the solvent-accessible side of the β-sheet is too distant from DNA to contribute any meaningful contacts with DNA. The first CXXC motif, including residues R71 and K72, is also too far away to interact with DNA, but the second CXXC is placed close to the DNA backbone with residues K78, R86, K89 and K91 having easy access to both the phosphates and the base pairs in the grooves. Although helix H3 contains six basic residues, residues K54, K57, and R58 are segregated at the extreme C-terminus of the helix (Figure 4b). Because of the width of the groove and the length of H3 in PF0610, these three residues are not close enough to contact DNA, but residues K42, K43, and K50 on H3 are within sufficient proximity to associate with DNA in both models. Another observation is that W1 of PF0610 is bulkier than W1 in most wHTH proteins. As a consequence, a number of steric clashes have been observed between the DNA backbone and the protein when modeling using the RFX1 and DP2 structures. In light of these clashes, the extra flexibility detected in the loop between the CXXC motifs in the relaxation-compensated CPMG experiment makes good sense as this allows the protein to adapt to the DNA backbone and reduces the energy of binding. Whether this has any bearing on the protein's biological function is uncertain.

Possible Biological Functions of PF0610. wHTH domains are found in proteins encoded in both prokaryotic and eukaryotic genomes. Most are believed to serve as DNA- or RNA-binding domains. A large number of wHTH proteins are transcriptional regulators, but wHTH-containing proteins that are involved in chromosome packing (for example, GH5) and DNA repair & modification (for example, CDC6 and DprA) also exist. There is even a wHTH domain in the RNA editing enzyme ADAR1. There are as yet no data on the role of PF0610 in *P. furiosus* metabolism, but we can discuss the possibilities based on the results of the structural and DNA binding work presented here.

Because of its apparent sequence-independent interaction with DNA, PF0610 could be a part of the chromatin system of *P. furiosus*. Archaea contain histone-like proteins that are highly similar to those from eukarya (*32*), and PF0610 might play a role not unlike that of the linker histone. There has also been much speculation regarding how *P. furiosus* maintains the structural integrity of its DNA at such a high ambient temperature (see ref *32*). Proteins unique to archaea, such as PF0610, might be crucial in making this possible. The numerous basic residues in PF0610 ensure strong interactions of the protein with DNA, and the Zn ribbon motif could help to improve the structural stability of the protein at a high temperature. On the other hand, DNA microarray analyses (*33*) indicated that PF0610 is expressed at a low basal level in *P. furiosus* cells, so the likelihood of PF0610 being a ubiquitous chromosomal protein is low.

Another possibility is that PF0610 is a metal-dependent transcription factor. Preliminary DNA microarray data show a significant increase in the level of expression of PF0610 when cells are grown on an iron-limited medium, suggesting that the protein may play a role in iron metabolism (A. L. Menon, unpublished data). Of necessity, the Zn form was used for NMR analysis; however, *E. coli* appears to be able to "insert" iron or zinc into this protein with equal efficiency, and its metal content reflects that of the medium. Precisely the same result was obtained with the production of *P. furiosus* rubredoxin in *E. coli* (*34*), a protein known to contain only iron in vivo. It therefore seems likely that PF0610 is an iron-containing protein. While the gel shift assay results suggested that the Zn form of PF0610 has an affinity for DNA that is independent of sequence, quantitative association constants for PF0610−DNA interactions were not obtained. Although it is possible that the interaction of PF0610 with DNA is nonspecific, it seems more likely that we failed to test its true target sequence, for which its affinity is much higher than what was seen in the assays. Since W1 of PF0610 is most likely disordered without the bound metal and given the DNA microarray data, our current hypothesis is that PF0610 is a ferrous iron sensor whose affinity for DNA is greatly reduced when the protein lacks the metal. It is anticipated that further analysis of the response of *P. furiosus* to iron limitation will identify regulatory DNA sequences that can be used as targets to investigate the binding of PF0610.

ACKNOWLEDGMENT

We thank Dr. Aaron Cowley (University of Georgia) for performing the analytical ultracentrifugation study on PF0610 as well as Dr. Fang Tian (Southeast Collaboratory on Biomolecular NMR) for collecting and analyzing the relaxation-compensated CPMG experiment and constructive discussions.

REFERENCES

1. Norvell, J., and Berg, J. M. (2005) The protein structure initiative, five years later, *Scientist 19*, 30−31.
2. Wang, B. C., Adams, M. W., Dailey, H., DeLucas, L., Luo, M., Rose, J., Bunzel, R., Dailey, T., Habel, J., Horanyi, P., Jenney, F. E., Jr., Kataeva, I., Lee, H. S., Li, S., Li, T., Lin, D., Liu, Z. J., Luan, C. H., Mayer, M., Nagy, L., Newton, M. G., Ng, J., Poole, F. L., II, Shah, A., Shah, C., Sugar, F. J., and Xu, H. (2005) Protein production and crystallization at SECSG: An overview, *J. Struct. Funct. Genomics 6*, 233−243.
3. Poole, F. L., II, Gerwe, B. A., Hopkins, R. C., Schut, G. J., Weinberg, M. V., Jenney, F. E., Jr., and Adams, M. W. (2005) Defining genes in the genome of the hyperthermophilic archaeon *Pyrococcus furiosus*: Implications for all microbial genomes, *J. Bacteriol. 187*, 7325−7332.
4. Altschul, S. F., Gish, W., Miller, W., Myers, E. W., and Lipman, D. J. (1990) Basic Local Alignment Search Tool, *J. Mol. Biol. 215*, 403−410.
5. Bernstein, F. C., Koetzle, T. F., Williams, G. J. B., Meyer, E. F., Brice, M. D., Rodgers, J. R., Kennard, O., Shimanouchi, T., and Tasumi, M. (1977) Protein Data Bank: Computer-Based Archival File for Macromolecular Structures, *J. Mol. Biol. 112*, 535−542.
6. Jones, D. T. (1999) GenTHREADER: An efficient and reliable protein fold recognition method for genomic sequences, *J. Mol. Biol. 287*, 797−815.
7. Wunderlich, Z., Acton, T. B., Liu, J. F., Kornhaber, G., Everett, J., Carter, P., Lan, N., Echols, N., Gerstein, M., Rost, B., and Montelione, G. T. (2004) The protein target list of the Northeast Structural Genomics Consortium, *Proteins 56*, 181−187.
8. Permi, P., Heikkinen, S., Kilpelainen, I., and Annila, A. (1999) Measurement of $^{1}J_{NC'}$ and $^{2}J_{HNC'}$ couplings from spin-state-selective two-dimensional correlation spectrum, *J. Magn. Reson. 140*, 32−40.
9. Loria, J. P., Rance, M., and Palmer, A. G. (1999) A TROSY CPMG sequence for characterizing chemical exchange in large proteins, *J. Biomol. NMR 15*, 151−155.
10. Millet, O., Loria, J. P., Kroenke, C. D., Pons, M., and Palmer, A. G. (2000) The static magnetic field dependence of chemical exchange linebroadening defines the NMR chemical shift time scale, *J. Am. Chem. Soc. 122*, 2867−2877.
11. Delaglio, F., Grzesiek, S., Vuister, G. W., Zhu, G., Pfeifer, J., and Bax, A. (1995) Nmrpipe: A Multidimensional Spectral Processing System Based on Unix Pipes, *J. Biomol. NMR 6*, 277−293.
12. Johnson, B. A., and Blevins, R. A. (1994) NMR View: A Computer-Program for the Visualization and Analysis of NMR Data, *J. Biomol. NMR 4*, 603−614.
13. Slupsky, C. M., Boyko, R. F., Booth, V. K., and Sykes, B. D. (2003) Smartnotebook: A semi-automated approach to protein sequential NMR resonance assignments, *J. Biomol. NMR 27*, 313−321.
14. Cornilescu, G., Delaglio, F., and Bax, A. (1999) Protein backbone angle restraints from searching a database for chemical shift and sequence homology, *J. Biomol. NMR 13*, 289−302.
15. Guntert, P., Mumenthaler, C., and Wuthrich, K. (1997) Torsion angle dynamics for NMR structure calculation with the new program DYANA, *J. Mol. Biol. 273*, 283−298.
16. Herrmann, T., Guntert, P., and Wuthrich, K. (2002) Protein NMR structure determination with automated NOE assignment using the new software CANDID and the torsion angle dynamics algorithm DYANA, *J. Mol. Biol. 319*, 209−227.
17. Schwieters, C. D., Kuszewski, J. J., Tjandra, N., and Clore, G. M. (2003) The Xplor-NIH NMR molecular structure determination package, *J. Magn. Reson. 160*, 65−73.
18. Day, M. W., Hsu, B. T., Joshuator, L., Park, J. B., Zhou, Z. H., Adams, M. W. W., and Rees, D. C. (1992) X-ray Crystal-Structures of the Oxidized and Reduced Forms of the Rubredoxin from the Marine Hyperthermophilic Archaebacterium *Pyrococcus furiosus*, *Protein Sci. 1*, 1494−1507.
19. Bau, R., Rees, D. C., Kurtz, D. M., Scott, R. A., Huang, H. S., Adams, M. W. W., and Eidsness, M. K. (1998) Crystal structure of rubredoxin from *Pyrococcus furiosus* at 0.95 angstrom resolution, and the structures of N-terminal methionine and formylmethionine variants of Pf Rd. Contributions of N-terminal interactions to thermostability, *J. Biol. Inorg. Chem. 3*, 484−493.
20. Blake, P. R., Day, M. W., Hsu, B. T., Joshuator, L., Park, J. B., Hare, D. R., Adams, M. W. W., Rees, D. C., and Summers, M. F. (1992) Comparison of the X-ray Structure of Native Rubredoxin from *Pyrococcus furiosus* with the NMR Structure of the Zinc-Substituted Protein, *Protein Sci. 1*, 1522−1525.
21. Aravind, L., Anantharaman, V., Balaji, S., Babu, M. M., and Iyer, L. M. (2005) The many faces of the helix-turn-helix domain: Transcription regulation and beyond, *FEMS Microbiol. Rev. 29*, 231−262.
22. Gajiwala, K. S., and Burley, S. K. (2000) Winged helix proteins, *Curr. Opin. Struct. Biol. 10*, 110−116.
23. MartinezHackert, E., and Stock, A. M. (1997) Structural relationships in the OmpR family of winged-helix transcription factors, *J. Mol. Biol. 269*, 301−312.
24. Aravind, L., and Koonin, E. V. (1999) DNA-binding proteins and evolution of transcription regulation in the archaea, *Nucleic Acids Res. 27*, 4658−4670.
25. Blake, P. R., Park, J. B., Zhou, Z. H., Hare, D. R., Adams, M. W. W., and Summers, M. F. (1992) Solution-State Structure by NMR of Zinc-Substituted Rubredoxin from the Marine Hyperthermophilic Archaebacterium *Pyrococcus furiosus*, *Protein Sci. 1*, 1508−1521.
26. Zhu, W. L., Zeng, Q. D., Colangelo, C. M., Lewis, L. M., Summers, M. F., and Scott, R. A. (1996) The N-terminal domain of TFIIB from *Pyrococcus furiosus* forms a zinc ribbon, *Nat. Struct. Biol. 3*, 122−124.
27. Clark, K. L., Halay, E. D., Lai, E. S., and Burley, S. K. (1993) Cocrystal Structure of the Hnf-3/Fork Head DNA-Recognition Motif Resembles Histone-H5, *Nature 364*, 412−420.
28. Brennan, R. G. (1993) The Winged-Helix DNA-Binding Motif: Another Helix-Turn-Helix Takeoff, *Cell 74*, 773−776.

29. Gajiwala, K. S., Chen, H., Cornille, F., Roques, B. P., Reith, W., Mach, B., and Burley, S. K. (2000) Structure of the winged-helix protein hRFX1 reveals a new mode of DNA binding, *Nature 403*, 916−921.
30. Zheng, N., Fraenkel, E., Pabo, C. O., and Pavletich, N. P. (1999) Structural basis of DNA recognition by the heterodimeric cell cycle transcription factor E2F-DP, *Gene Dev. 13*, 666−674.
31. Holm, L., and Sander, C. (1994) Searching Protein-Structure Databases Has Come of Age, *Proteins: Struct., Funct., Genet. 19*, 165−173.
32. Topping, T. B., and Gloss, L. M. (2004) Stability and folding mechanism of mesophilic, thermophilic and hyperthermophilic archaeal histones: The importance of folding intermediates, *J. Mol. Biol. 342*, 247−260.
33. Schut, G. J., Brehm, S. D., Datta, S., and Adams, M. W. (2003) Whole-genome DNA microarray analysis of a hyperthermophile and an archaeon: *Pyrococcus furiosus* grown on carbohydrates or peptides, *J. Bacteriol. 185*, 3935−3947.
34. Eidsness, M. K., Richie, K. A., Burden, A. E., Kurtz, D. M., Jr., and Scott, R. A. (1997) Dissecting contributions to the thermostability of *Pyrococcus furiosus* rubredoxin: β-Sheet chimeras, *Biochemistry 36*, 10406−10413.

BI061870H